

Probing small neutron skin variations in isotope pairs by hyperon-antihyperon production in antiproton–nucleus interactions

Falk Schupp,¹ Josef Pochodzalla,^{1, 2, 3,*} Michael Böltting,¹ Martin Christiansen,¹ Theodoros Gaitanos,⁴ Horst Lenske,⁵ and Marcell Steinen¹

¹Helmholtz-Institut Mainz, Johannes Gutenberg-Universität Mainz, 55099 Mainz, Germany

²Institute für Kernphysik, Johannes Gutenberg-Universität Mainz, 55099 Mainz, Germany

³PRISMA⁺ Cluster of Excellence, Johannes Gutenberg-Universität Mainz, 55099 Mainz, Germany

⁴Department of Theoretical Physics, Aristotle University of Thessaloniki, GR-54124 Thessaloniki, Greece

⁵Institut für Theoretische Physik, Justus-Liebig-Universität Gießen, D-35392 Gießen, Germany

(Dated: November 22, 2024)

We propose a new method to measure the evolution of the neutron skin thickness between different isotopes with small statistical and systematic uncertainties. We consider antiproton–nucleus interactions close to the production threshold of $\Lambda\bar{\Lambda}$ and $\Sigma^-\bar{\Lambda}$ pairs. At low energies, $\Lambda\bar{\Lambda}$ pairs are produced in $\bar{p} + p$ collisions, while $\Sigma^-\bar{\Lambda}$ pairs can only be produced in $\bar{p} + n$ interactions. Within a simple geometrical picture we show that the double ratio for the production of $\Sigma^-\bar{\Lambda}$ and $\Lambda\bar{\Lambda}$ pairs for two different isotopes are directly related to the variation of the neutron skin thickness between the two nuclei. Performing high statistics calculations with the Gießen Boltzmann–Uehling–Uhlenbeck (GiBUU) transport model for several isotope pairs covering a wide range of elements we verify a strong correlation between the double ratio from the full transport simulations and the schematic model. This correlation enables us to quantify the high potential of the proposed method for precise studies of neutron skin variations in isotope chains.

I. INTRODUCTION

To describe neutron rich matter which eventually appears in dense stellar objects, knowledge on the isospin part of the EoS is indispensable. Luckily, the isospin dependence of the EoS correlates strongly with the distribution of neutrons in nuclei, see [1–3] and references therein. Thus the thickness of neutron skins in nuclei impacts our knowledge on the structure of neutron stars [4–11]. Furthermore, the evolution of the neutron skin and proton distributions along isotope chains provide important information for our understanding of the nuclear structure over the whole nuclear chart [12–18].

The neutron skin thickness, ΔR_{np} , is usually defined as the difference between the root-mean-squared (rms) point radii of the neutron and proton density distributions. However, this definition is not unique because of possibly significant density variations both, in the nuclear periphery and in the center [19]. Since quantal shell effects also influence the nucleon distributions, the focus of their studies often lies on neutron rich doubly magic nuclei, like ^{40}Ca , ^{48}Ca and ^{208}Pb .

Experimentally charge distributions, which mainly reflects the proton distribution, can be explored by electromagnetic probes like electrons or muons rather precisely. On the other hand, accurate information on neutron radii and neutron skins is scarce. Experimental techniques to determine the neutron distributions of nuclei using strongly interacting probes range from proton elastic [21, 26–29] and inelastic [30, 31] reactions, measurement of interaction cross section of heavy nuclei [12, 17, 21, 32–34] and antiproton interactions [35]. The electric dipole response can be studied by α particle scattering exciting the giant dipole resonance [36, 37], the excitation of the pigmy dipole resonance [38] and spin-dipole resonance

[37, 39], the electric dipole polarizability [40, 41], pion scattering [15], coherent pion photoproduction [42], antiprotonic x-rays [16, 43]. The parity-violating electron scattering asymmetry provides a measure of the weak charge distribution and hence of neutron distribution in appropriate nuclei [20]. Finally, since neutron star properties and the neutron skins of nuclei are highly related [3], also astrophysical observations of neutron stars provide in an indirect way constraints on the neutron skin of e.g. ^{208}Pb [44–46]. Despite these many experimental opportunities, the neutron distributions still carry considerable systematic uncertainties, see, for instance the discussions in Refs. [8, 37, 47].

Calcium isotopes are of particular value, since for such medium heavy nuclei, already accurate *ab initio* calculations are possible [48–50], although in many cases a quantitative reproduction of nuclear radii is still an open issue [51, 52]. Calculations using a wide variety of EoS’s show a remarkable correlation between the slope parameter of the symmetry energy and the neutron skin thickness of ^{48}Ca or ^{208}Pb . As consequence there exists a rather model independent correlation between the neutron skin thickness of these two nuclei [20–22] (see also in the upper right panel of Figure 1). Data available for the two doubly magic nuclei ^{48}Ca and ^{208}Pb are exemplified in the left and lower panel in Figure 1, respectively. Many of these analyses have sizable systematic uncertainties since the analyses are model dependent (for a recent analysis see e.g. [53, 54]). In this figure, statistical and systematic uncertainties (if available) were added in quadrature. Detailed information on the displayed data are listed in Table III and Table IV in the Appendix.

A rather clean measure of the neutron distribution with small systematic uncertainties is expected from the electroweak asymmetry in elastic electron-nucleus scattering [20]. However, the PREX measurement of ^{208}Pb [23, 24] and the CREX result for ^{48}Ca [25] are in tension with the expected correlation between the neutron skin of ^{48}Ca and ^{208}Pb shown

* Contact author:pochodza@uni-mainz.de

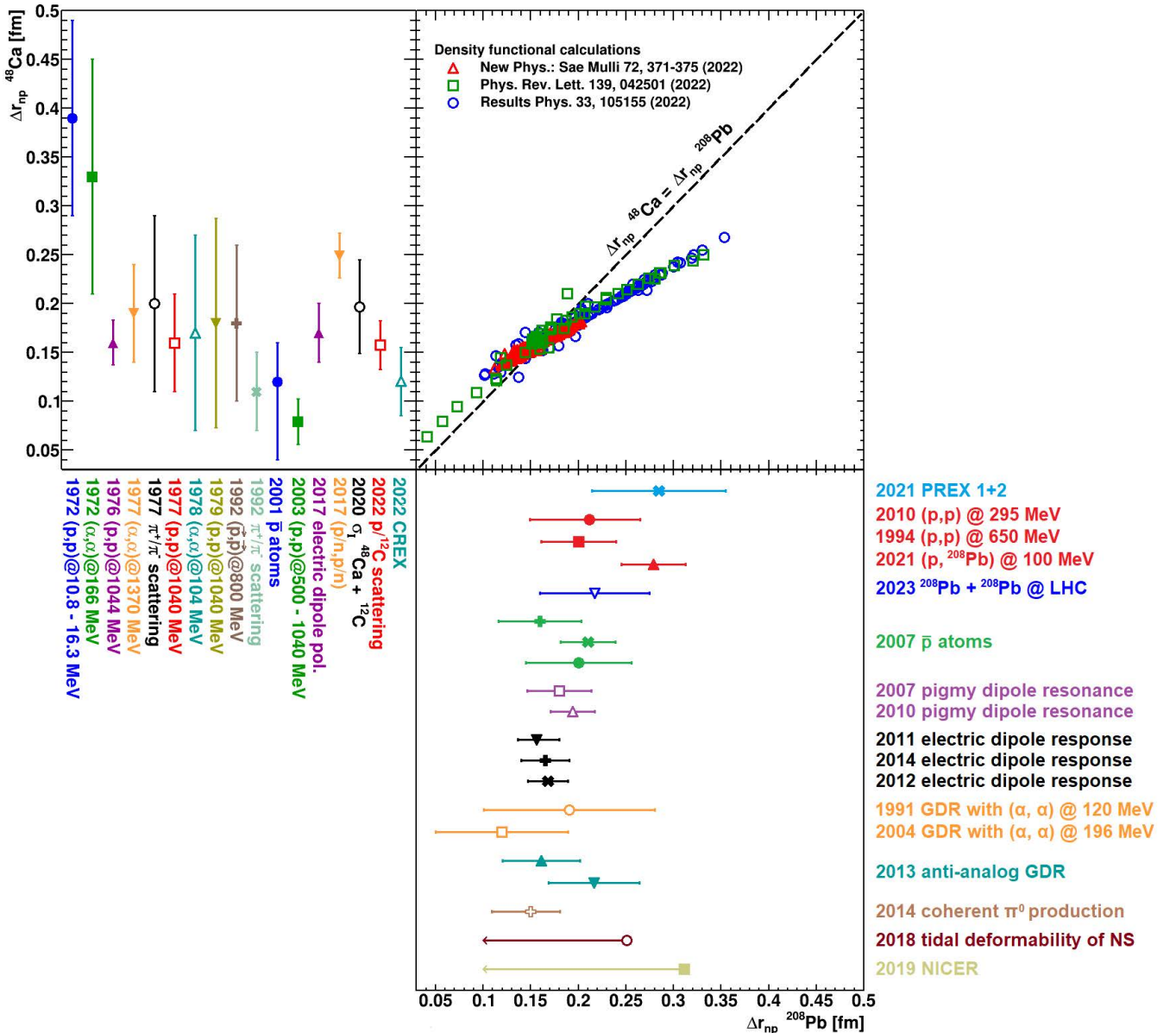


FIG. 1. Experimental values for the neutron skin thickness of the doubly magic nuclei ^{48}Ca (left panel) and ^{208}Pb (lower right panel). Detailed information on the displayed data are listed in Table III and Table IV. The upper right panel shows the relation between the neutron skin thickness of ^{48}Ca or ^{208}Pb predicted by various models with different EoS [20–22]. Note, that the combined PREX measurement of ^{208}Pb [23, 24] and the CREX result for ^{48}Ca [25] are in tension with these model predictions. References are listed in the Appendix.

in the upper right panel of Figure 1. Indeed, for example a recent nonlocal dispersive optical model analysis suggests a neutron skin for ^{208}Pb of $0.18^{+0.07}_{-0.06}$ fm [54], which is significantly lower than the PREX result and for ^{48}Ca a skin of $0.22^{+0.02}_{-0.03}$ fm, which in turn is significantly larger than the CREX value. This situation clearly calls for further detailed theoretical [55] as well as improved experimental studies.

In this work we present a novel method to explore the variation of the neutron skin between two different isotopes of a given element with high precision and accuracy. For that purpose we consider antiproton–nucleus interactions close to the thresholds of $\Lambda\bar{\Lambda}$ and $\Sigma^-\bar{\Lambda}$ pair production. At low energies,

$\Lambda\bar{\Lambda}$ pairs are produced in $\bar{p}+p$ collisions, while $\Sigma^-\bar{\Lambda}$ pairs can only be produced in $\bar{p}+n$ interactions. Unlike other probes, antiprotons are strongly absorbed in the nuclear periphery and, therefore, are particularly sensitive to small variations of the nuclear skin.

Measuring the probabilities $p_{\Lambda\bar{\Lambda}}$ and $p_{\Sigma^-\bar{\Lambda}}$ for the two processes for a reference isotope (I) and a second isotope (II), allows to determine the double ratio

$$DR = \frac{p_{\Sigma^-\bar{\Lambda}}^{II}/p_{\Lambda\bar{\Lambda}}^{II}}{p_{\Sigma^-\bar{\Lambda}}^I/p_{\Lambda\bar{\Lambda}}^I}. \quad (1)$$

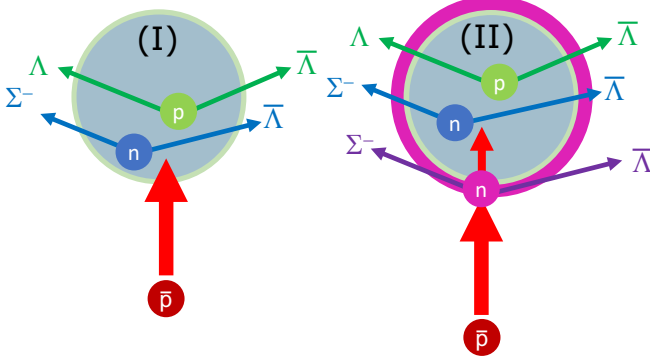


FIG. 2. Illustration of the production of $\Lambda\bar{\Lambda}$ and $\Sigma^-\bar{\Lambda}$ pairs in antiproton-nucleus interactions. We consider two isotopes (I) and (II) which differ by an additional outer neutron layer with thickness Δ_n , shown in pink. The production yields for the two different hyperon-antihyperon pairs provide a measurement of the effective thickness of this additional neutron layer.

Such a double ratio does not require the absolute determination of cross sections and also the different energy dependence for the $\Lambda\bar{\Lambda}$ and $\Sigma^-\bar{\Lambda}$ channels is eliminated. Furthermore, measuring both the production probabilities for a given isotope simultaneously, many experimental uncertainties cancel or can be significantly reduced.

Within a simple geometrical picture for central collisions we first show in section II that this ratio is strongly related to the difference of the neutron skin thicknesses of the two considered isotopes (I) and (II) depicted in Figure 2.

In section III we present a schematic scenario to describe the full impact parameter range.

Finally, we explore in section IV this ratio with the Gießen Boltzmann–Uehling–Uhlenbeck (GiBUU) transport model for different isotopes. Using the neutron distributions which describe the initial state in these GiBUU simulations, we find a remarkable correlation between double ratio predicted by the simple picture of section III and the double ratio predicted by the complete GiBUU simulations. As a consequence, the simple scenario presented in section III enables us to explore the sensitivity of the double ratio to variations of the neutron distributions. As a possible application at the \bar{p} ANDA experiment, we perform a systematic study for the case of ^{40}Ca and ^{48}Ca .

II. MOTIVATION OF THE METHOD: A SIMPLE SCENARIO

Because of the strong absorption of antiprotons in nuclei the production of hyperon–antihyperon pairs happens in the nuclear periphery. For simplicity we consider a nearly central antiproton–nucleus collision (see left part of Figure 2). Close to threshold, the probability $p_{\Lambda\bar{\Lambda}}^I$ to produce a $\Lambda\bar{\Lambda}$ pair within the reference nucleus (I) can be written as

$$p_{\Lambda\bar{\Lambda}}^I = \kappa_{\Lambda\bar{\Lambda}} \cdot \frac{\rho(p)}{\rho(p) + \rho(n)} \cdot \frac{\sigma_{\Lambda\bar{\Lambda}}}{\sigma_{\text{tot}}}. \quad (2)$$

Here σ_{tot} denotes the total $\bar{p} + A$ cross section and $\sigma_{\Lambda\bar{\Lambda}}$ is the elementary $\bar{p} + p \rightarrow \Lambda\bar{\Lambda}$ cross section. $\rho(p)$ and $\rho(n)$ denote the densities in the periphery of the target nucleus of protons and neutrons, respectively.

The factor $\kappa_{\Lambda\bar{\Lambda}}$ describes the loss of $\Lambda\bar{\Lambda}$ pairs due to absorptive re-scattering. Similarly, the production probability of $\Sigma^-\bar{\Lambda}$ pairs can be approximated by

$$p_{\Sigma^-\bar{\Lambda}}^I = \kappa_{\Sigma^-\bar{\Lambda}} \cdot \frac{\rho(n)}{\rho(p) + \rho(n)} \cdot \frac{\sigma_{\Sigma^-\bar{\Lambda}}}{\sigma_{\text{tot}}}. \quad (3)$$

Because of the large annihilation cross section of antibaryons in nuclei, both, $\kappa_{\Lambda\bar{\Lambda}}$ and $\kappa_{\Sigma^-\bar{\Lambda}}$ are dominated by the $\bar{\Lambda}$ absorption. Therefore, we assume $\kappa_{\Lambda\bar{\Lambda}} \approx \kappa_{\Sigma^-\bar{\Lambda}} \equiv \kappa_I$.

We now turn to a isotope (II) with a larger neutron number and hence a more extended neutron distribution. For simplicity, we assume that the proton distribution remains identical to the one of nucleus (I) and that the neutron distribution is only extended by an additional halo Δ_n at the surface, see pink area in the right part of Figure 2. Such a situation is approximately found in isotope chains of heavy nuclei. In such a scenario, the production of $\Lambda\bar{\Lambda}$ pairs is reduced by the absorption probability p_{abs} of the incident antiprotons within this additional neutron skin Δ_n :

$$p_{\Lambda\bar{\Lambda}}^{II} = (1 - p_{\text{abs}}) \cdot \kappa_{II} \cdot \frac{\rho(p)}{\rho(p) + \rho(n)} \cdot \frac{\sigma_{\Lambda\bar{\Lambda}}}{\sigma_{\text{tot}}}. \quad (4)$$

The absorption probability p_{abs} can be expressed in terms of the total $\bar{p} + n$ reaction cross section $\sigma_{\bar{p}n}$ [63] and the integrated skin density $\int_{\Delta_n} \rho_n dr_n$ of the additional neutron skin of nucleus (II) with respect to the reference nucleus (I):

$$1 - p_{\text{abs}} \approx \exp \left\{ - \sigma_{\bar{p}n} \cdot \int_{\Delta_n} \rho_n dr_n \right\} \quad (5)$$

Like the incoming antiprotons, the produced $\bar{\Lambda}$ are also absorbed in the additional neutron layer. We use the factorisation ansatz $\kappa_{II} = \kappa_I \cdot \kappa_n$. With this simplification we can express Equation 4 as

$$p_{\Lambda\bar{\Lambda}}^{II} = \kappa_n \cdot (1 - p_{\text{abs}}) \cdot p_{\Lambda\bar{\Lambda}}^I. \quad (6)$$

The production of $\Sigma^-\bar{\Lambda}$ pairs gains an additional component from the additional neutron skin. On the other hand, the contribution from the inner part of the nucleus (II) is reduced by the loss of antiprotons in the additional neutron layer:

$$\begin{aligned} p_{\Sigma^-\bar{\Lambda}}^{II} &= \kappa_{II} \cdot p_{\text{abs}} \cdot \frac{\sigma_{\Sigma^-\bar{\Lambda}}}{\sigma_{\text{tot}}} \\ &\quad + (1 - p_{\text{abs}}) \cdot \kappa_{II} \frac{\rho(n)}{\rho(p) + \rho(n)} \cdot \frac{\sigma_{\Sigma^-\bar{\Lambda}}}{\sigma_{\text{tot}}}. \end{aligned} \quad (7)$$

Here, we assume that the loss of outgoing Σ^- and/or $\bar{\Lambda}$ for pairs produced in the additional neutron skin is the same as for pairs produced within the core nucleus. We thus obtain for the double ratio

$$DR = \frac{p_{\Sigma^-\bar{\Lambda}}^{II}/p_{\Lambda\bar{\Lambda}}^{II}}{p_{\Sigma^-\bar{\Lambda}}^I/p_{\Lambda\bar{\Lambda}}^I} = \frac{p_{\text{abs}} \cdot \frac{\rho(p) + \rho(n)}{\rho(n)} + (1 - p_{\text{abs}})}{1 - p_{\text{abs}}} \quad (8)$$

isotope	abundance	exp. charge radius R_p^{exp} [fm]	proton radius R_p [fm]	neutron radius R_n [fm]	neutron skin ΔR_{pn} [fm]	skin difference Δ_n [fm]	RMF model
	[%]						
^{20}Ne	90.5	2.992 ± 0.008 [56]	2.782	2.758	-0.024	-	NL3 [57]
^{22}Ne	9.3	2.986 ± 0.021 [56]	2.800	2.887	0.087	0.111	NL3 [57]
^{40}Ca	96.9	3.4776 ± 0.0019 [58]	3.452	3.416	-0.036	-	NL1 [57]
^{48}Ca	0.187	3.4786 ± 0.0106 [58, 59]	3.525	3.731	0.206	0.242	NL1 [57]
^{40}Ca	96.9	3.4776 ± 0.0019 [58]	3.391	3.354	-0.037	-	NL3 [57]
^{48}Ca	0.187	3.4786 ± 0.0106 [58, 59]	3.472	3.659	0.187	0.224	NL3 [57]
^{40}Ca	96.9	3.4776 ± 0.0019 [58]	3.396	3.360	-0.036	-	NL3* [60]
^{48}Ca	0.187	3.4786 ± 0.0106 [58, 59]	3.475	3.666	0.191	0.227	NL3* [60]
^{58}Ni	68.1	3.770 ± 0.002 [61]	3.769	3.768	0.000	-	NL3 [57]
^{64}Ni	0.926	3.854 ± 0.002 [61]	3.822	3.947	0.125	0.125	NL3 [57]
^{129}Xe	26.4	4.7775 ± 0.0050 [58]	4.768	4.932	0.164	-	NL3 [57]
^{130}Xe	4.1	4.7818 ± 0.0049 [58]	4.776	4.950	0.174	0.010	NL3 [57]
^{131}Xe	21.2	4.7808 ± 0.0049 [58]	4.784	4.968	0.184	0.020	NL3 [57]
^{132}Xe	26.9	4.7859 ± 0.0048 [58]	4.792	4.986	0.194	0.030	NL3 [57]
^{134}Xe	10.4	4.7899 ± 0.0047 [58]	4.809	5.023	0.213	0.049	NL3 [57]
^{136}Xe	8.9	4.7964 ± 0.0047 [58]	4.826	5.059	0.233	0.069	NL3 [57]

TABLE I. Isotopes studied in this work. The second and third column give the natural abundances and the experimental charge radii. Proton and neutron rms radii and their differences predicted by the relativistic mean field model of Ref. [57] for stable or long-lived isotopes are listed in the column 4 to 7. The radial distributions are generated during the initialization of the Gießen Boltzmann–Uehling–Uhlenbeck (GiBUU) transport model simulations [62].

With the simplifying assumption $\rho(p) = \frac{Z}{N} \cdot \rho(n)$, where Z denotes the element number and N the average neutron number of the two isotopes, we finally find for the double ratio the expression

$$DR = \frac{1 + p_{\text{abs}} \cdot Z/N}{1 - p_{\text{abs}}} \quad (9)$$

Since the variation of the neutron skin thickness is rather small, the additional absorption probability p_{abs} is also small. In this case, we can expand Equation 9 and obtain a linear relation between the double ratio DR and the absorption probability of the incident antiprotons within the increased neutron skin Δ_n .

$$DR \approx 1 + \left(1 + \frac{Z}{N}\right) \cdot p_{\text{abs}}. \quad (10)$$

This expression is nearly independent of the considered nuclei and it signals that DR is a direct measure of the increment of (integrated) neutron skin thickness. The only quantity to be known is the total $\bar{p} + n$ reaction cross section $\sigma_{\bar{p}n}$ which can be determined from experiment by comparing e.g. $\bar{p}p$ and $\bar{p}d$ interactions.

III. FINITE IMPACT PARAMETER RANGE

Of course, this simplified geometrical picture has several deficiencies:

- In \bar{p} -A collisions one can not constrain the impact parameter and one, therefore, has to consider the full impact parameter range.

- Usually incident antiprotons do not traverse the skin radially and the absorption probability depends on the impact parameter.
- The absorption of produced antihyperons favor the pair production in peripheral reactions.
- Different isotopes may also have different proton distributions.

Because of the large absorption cross section for antiprotons, the production ratios for $\Sigma^- \bar{\Lambda}$ and $\Lambda \bar{\Lambda}$ pairs is expected to reflect the neutron and proton content of the nuclear periphery and will, therefore, be strongly related to the neutron skin. However, one has to keep in mind that at threshold also the beam energy influences this ratio because of the different masses of the produced hyperons. Considering the ratios for two isotopes by the double ratio, this influence largely cancels.

In this work we consider an incident \bar{p} momentum of 2.4 GeV/c. At this energy, the interaction cross sections of $\bar{p}+p$ and $\bar{p}+n$ are similar in magnitude and about 55 mb [63]. For such a cross section, the interaction length at normal nuclear density is about 1.14 fm, corresponding to an integrated areal density along the antiproton path of $\int_{\Delta} \rho_{n+p} dz \approx 0.18 \text{ fm}^{-2}$.

The density distributions used in the following are generated during the initialization of the GiBUU simulations using the RMF parameter set of Ref. [57]. Assuming for simplicity a straight line trajectory along the z-direction for the incident antiproton, Figure 3 shows the areal density $\rho_{\Delta}^{p,n} = \int_{\Delta} \rho_{n,p} dz$ for protons (red lines) and neutrons (blue lines) along the antiproton path within one interaction length Δ for ^{40}Ca (dashed lines) and ^{48}Ca (solid lines) as a function of the impact parameter. Whereas for ^{40}Ca the proton and neutron content within

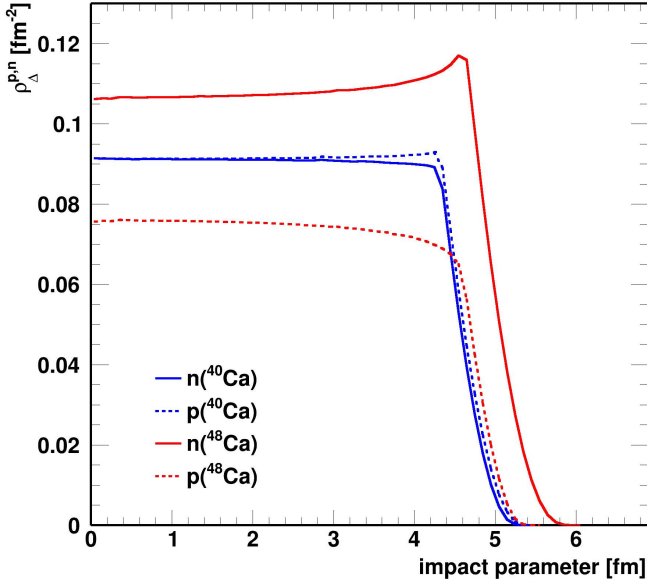


FIG. 3. Fractions of protons (dashed lines) and neutrons (solid lines) within one interaction length for ^{40}Ca (blue lines) and ^{48}Ca (red lines) at an incident momentum of $2.4 \text{ GeV}/c$ according to section III. The density distributions were generated during the initialization of the Gießen Boltzmann–Uehling–Uhlenbeck (GiBUU) transport model simulations [62] using the RMF parameter set of Ref. [57].

Δ is rather similar, for ^{48}Ca the neutrons exceed the protons by more than 50%. Integrating over all impact parameters, one finds for this case a neutron-to-proton ratio of 0.97 and 1.65 for ^{40}Ca and ^{48}Ca , respectively. The expected double ratio amounts to 1.70. The last column in Table II lists the double ratios expected for all studied isotope pairs and different RMF parameters from this schematic scenario.

To illustrate the sensitivity of the method in case of only small variations of the neutron distribution, we explore here first the isotope chain of xenon. At an antiproton storage ring, xenon can be experimentally explored in the mass range from $A = 129$ to $A = 136$. Of course, one has to keep in mind, that an efficient gas recirculation system will be mandatory. The filled red squares and blue points in Figure 4 show the rms radii of the proton and neutron distributions as a function of the Xe mass number. In these calculations not only the neutron radii but, unlike in the simple geometrical picture presented above also the proton radii are rising slightly with increasing neutron number. This increasing charge radius is qualitatively consistent with experimental data, see open squares in Figure 4 [58], though the experimental slope with the mass number is only about half as large. Note that the range of the neutron skin varies by only 0.13 fm, which is only a factor of two larger as the uncertainty of the PREX measurement for Pb. Since parity violating e^- scattering is generally hampered by limited statistics, exploring such small neutron skin variation in heavy isotope chains clearly calls for alternative methods.

Figure 5 shows the double ratio from the two simplified

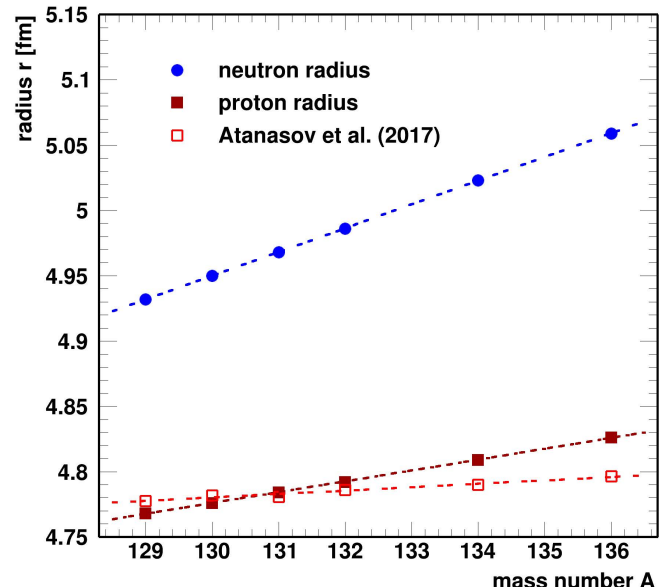


FIG. 4. Proton (filled red squares) and neutron (blue points) rms radii of the initial distributions for stable or long-lived xenon isotopes used by the GiBUU simulations [62]. The open red squares show experimental values for the proton radii [58, 64]. The lines are drawn to guide the eye.

scenarios in section II (blue squares) and section III (green dots) for xenon isotopes with mass $A=130-136$ with respect to ^{129}Xe . Compared to the simple analytic expression of Equation 9 with zero impact parameter, the ratio is significantly enhanced by considering the full impact parameter range. This is caused by the larger role played by the neutron rich nuclear periphery at large impact parameters. Within this picture a significant variation of the double ratio over such an isotope chain is expected.

IV. GIBUU TRANSPORT STUDY

A more realistic description of the hyperon pair production can be achieved by microscopic transport calculations. One such model, the Giessen Boltzmann-Uehling-Uhlenbeck (GiBUU) transport model [62], describes many features of \bar{p} -nucleus interactions in the FAIR energy range [62, 65, 66]. Particularly the presently available data on strangeness production are well reproduced. These simulations also avoid the approximations adopted in the derivation of Equation 9. In future studies we will also consider the co-planarity of the produced hyperon-antihyperon pair to extract additional information. However, in the present work we restrict the discussion to the total production ratios.

In the following, we employ the GiBUU model to study $\bar{p} + \text{Ne}, \text{Ca}, \text{Ni}$, and Xe reactions of several isotopes. All studied isotopes have a sizable abundance (Table I) and can in principle be used for experimental studies. The simulations were performed with an incident antiproton momentum of $2.4 \text{ GeV}/c$.

target	RMF model	events [10^6]	number of pairs	GiBUU	double ratio Equation 9	ρ_Δ (section III)
^{20}Ne	NL3 [57]	167	32387	10870	—	—
^{22}Ne	NL3 [57]	171	29227	13297	1.356 ± 0.021	1.110
^{40}Ca	NL1 [57]	415	76323	22880	—	—
^{48}Ca	NL1 [57]	450	66694	36074	1.799 ± 0.018	1.238
^{40}Ca	NL3 [57]	415	74280	21827	—	—
^{48}Ca	NL3 [57]	450	61313	32391	1.798 ± 0.019	1.219
^{40}Ca	NL3* [60]	415	78753	23438	—	—
^{48}Ca	NL3* [60]	450	64212	34523	1.807 ± 0.018	1.222
^{58}Ni	NL3 [57]	100	16811	5230	—	—
^{64}Ni	NL3 [57]	108	14978	6534	1.402 ± 0.030	1.120
^{129}Xe	NL3 [57]	109	13717	6238	—	—
^{130}Xe	NL3 [57]	109	13394	6225	1.022 ± 0.022	1.009
^{131}Xe	NL3 [57]	109	13403	6379	1.047 ± 0.023	1.017
^{132}Xe	NL3 [57]	109	13335	6556	1.081 ± 0.023	1.026
^{134}Xe	NL3 [57]	109	12771	6656	1.146 ± 0.025	1.042
^{136}Xe	NL3 [57]	109	12680	6739	1.169 ± 0.025	1.170

TABLE II. Number of generated inclusive interactions and production yield of $\Lambda\bar{\Lambda}$ and $\Sigma^-\bar{\Lambda}$ pairs in \bar{p} -Ne, Ca, Ni and Xe interactions at an incident momentum of 2.4 GeV/c. The last three columns show the double ratios deduced from the GiBUU simulation, and the simple models presented in section II and section III.

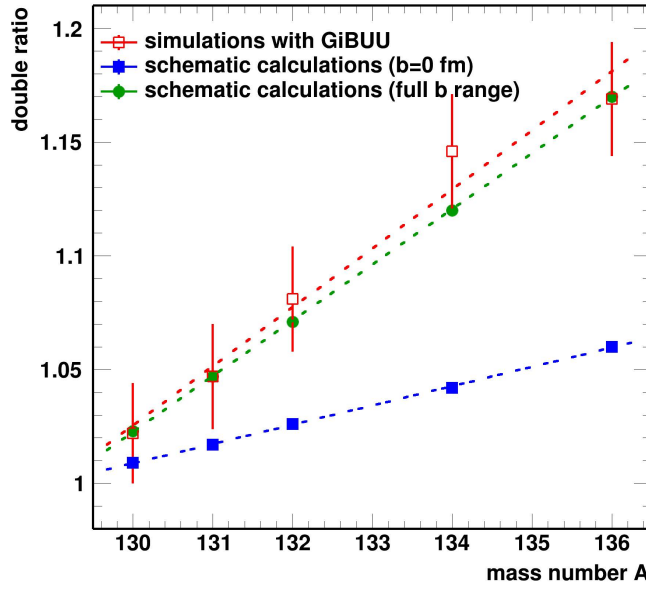


FIG. 5. Double ratio predicted from the two simplified scenarios in section II (blue squares) and section III (green dots) for different xenon isotopes of mass $A=130-136$ with respect to ^{129}Xe . The density distributions were generated during the initialization of the Gießen Boltzmann–Uehling–Uhlenbeck (GiBUU) transport model simulations [62] using the RMF parameter set of Ref. [57]. The red circlesshow the results of the GiBUU simulations. The lines are drawn to guide the eye.

The number of generated events for each nucleus are listed in Table II. Typically, 100 million events require a computational time of about four days on the MOGON2 high performance computing cluster at the University of Mainz. During the initialization of these simulations, the proton and neutron

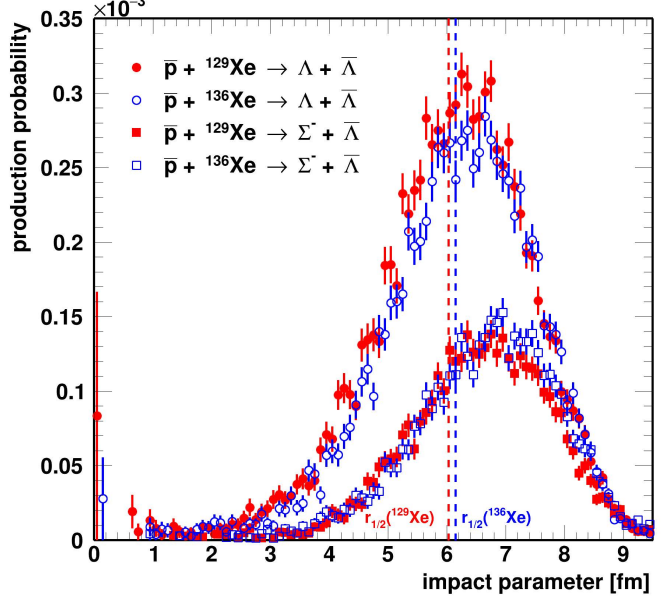


FIG. 6. Production probability of $\Lambda\bar{\Lambda}$ pairs (circles) and $\Sigma^-\bar{\Lambda}$ pairs (squares) produced exclusively in 2.4 GeV/c \bar{p} - ^{129}Xe (red symbols) and \bar{p} - ^{136}Xe (blue symbols) interactions as a function of the impact parameter. For orientation, the two lines mark the half-density radii $r_{1/2}$ of ^{129}Xe (red line) and \bar{p} - ^{136}Xe (blue line).

distributions of the target nuclei are generated by a self consistent relativistic mean-field (RMF) model. If not mentioned otherwise, we use the RMF parameter set of Ref. [57].

A. The case of xenon isotope chain

Figure 6 shows the predicted production probability $\sim b^{-1} dN_{Y\bar{\Lambda}}/db$ for $\Lambda\bar{\Lambda}$ pairs (circles) and $\Sigma^-\bar{\Lambda}$ pairs (squares) as a function of the impact parameter b for ^{129}Xe (red) and ^{136}Xe (blue) interactions. The vertical dashed lines indicates rms-radii for neutrons and protons of ^{129}Xe (red) and ^{136}Xe (blue; see Table I). As expected, the pair production probability is largest in the nuclear periphery, where the chance for both, the $\bar{\Lambda}$ and the Λ or Σ^- to escape, is sizable. At very small impact parameters particularly the forward going $\bar{\Lambda}$ have to cross a large part of the target nucleus to be emitted. Consequently, for heavy nuclei like xenon the absorption probability for $\bar{\Lambda}$ approaches 1 for more central collisions.

Figure 7 shows the ratio of exclusive $\Lambda\bar{\Lambda}$ (red symbols) and $\Sigma^-\bar{\Lambda}$ pair (blue symbols) production in ^{136}Xe vs. ^{129}Xe nuclei as a function of the impact parameter. At impact parameters around the nuclear radius, the $\Lambda\bar{\Lambda}$ production in $\bar{p} + p$ interactions is reduced for the more neutron rich isotope due to the more extended neutron skin which leads to an enhanced absorption for the incoming \bar{p} as well as the outgoing $\bar{\Lambda}$. At very large impact parameters beyond >7 fm, and at hence low matter density, the antiprotons are hardly absorbed and the antiprotons pass the full proton (and neutron) distributions. Since the proton distributions are quite similar for the two isotopes, the $\Lambda\bar{\Lambda}$ ratio approaches 1.

The production ratio for $\Sigma^-\bar{\Lambda}$ pairs indicated by blue symbols in Figure 7 shows a somewhat different impact parameter dependence. For $\Sigma^-\bar{\Lambda}$ production, the absorptions of the incident antiprotons and the produced $\bar{\Lambda}$ within an extended neutron skin act in opposite direction. Indeed, a weak suppression is observed at more central collisions and the region of intermediate impact parameters shows similar yields for ^{129}Xe and ^{136}Xe . However, going further into the low density periphery of the nuclei beyond $b > 6$ fm, the absorption of the $\bar{\Lambda}$ is less important and the additional neutron content of ^{136}Xe enhances the $\Sigma^-\bar{\Lambda}$ production with respect to ^{129}Xe considerably.

Table II gives the individual yields for all six isotopes and the yield ratios between $^{130}\dots^{136}\text{Xe}$ and ^{129}Xe . Already the individual yields show a continuous sensitivity to the additional neutron layer in ^{136}Xe . Since the yield ratios R for $\Lambda\bar{\Lambda}$ and $\Sigma^-\bar{\Lambda}$ pairs are affected in opposite directions, the sensitivity is even more enhanced by forming the double ratio $R(\Lambda\bar{\Lambda})/R(\Sigma^-\bar{\Lambda})$.

It is interesting to note, that the double ratio from the GiBUU simulations (red squares in Figure 5) and the ratios from our simplified calculations of section III (green squares in Figure 5) agree within errors. Although the quantitative agreement may be fortuitous, this strong correlation shows that the simple analytic model outlined in section III covers the main features of the process. This will be discussed in more detail in section V.

B. The case of ^{20}Ne and ^{22}Ne

Like the noble gas xenon, also neon is a conceivable element for the PANDA cluster-jet target. Besides the common ^{20}Ne , also ^{22}Ne might be a feasible target if the cluster target system is equipped with a gas regeneration system. The measured charge radii of ^{20}Ne ($r_c=2.992\pm 0.008$ fm) and ^{22}Ne ($r_c=2.986\pm 0.021$ fm) differ only very little [56]. This small variation is also reproduced by Hatree-Fock-Bogoliubov [67] and relativistic mean field calculations [68]. On the other hand according to these calculations, the radius of the neutron distribution of ^{22}Ne is about 0.2 fm wider than the one of ^{20}Ne [67]. The RMF model implemented in the GiBUU code gives a difference which is about half as large (see Table I)

The upper part of Table II gives the individual yields and the yield ratios for ^{22}Ne and ^{20}Ne targets predicted by GiBUU for an incident antiproton momentum of 2.4 GeV/c. Unlike for the xenon isotopes, already the individual yields show a remarkable sensitivity to the additional neutron layer in ^{22}Ne . Since the yield ratios for $\Lambda\bar{\Lambda}$ and $\Sigma^-\bar{\Lambda}$ -pairs are affected in opposite directions by the additional neutron layer, the sensitivity is even more enhanced by forming the double ratio DR, which reaches a value around 1.4.

C. The case of ^{40}Ca and ^{48}Ca

Charge radii of calcium isotopes are very well known [69]. Indeed, ^{48}Ca has the same rms charge radius as ^{40}Ca within $0.001\pm 0.003(\text{stat.})\pm 0.010(\text{syst.})$ fm [59], making this isotope pair an ideal case for the proposed method. One has to keep in mind though, that the proton density distributions also show significant differences [70, 71].

The GiBUU model evaluates the initial charge and neutron distributions of the target nucleus with a specified RMF pa-

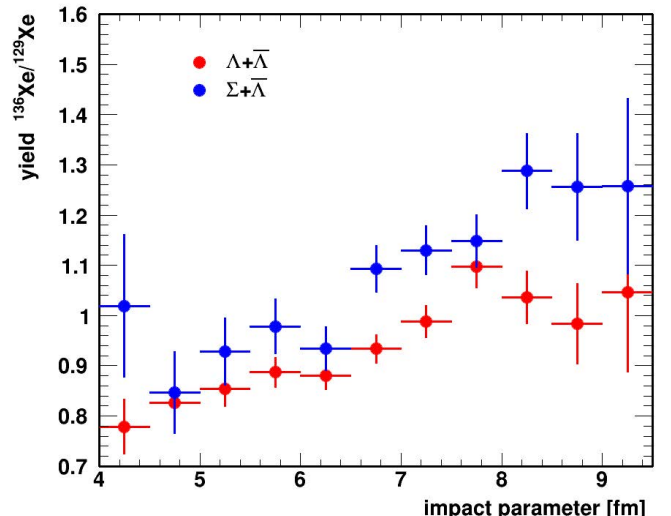


FIG. 7. Ratio of exclusive $\Lambda\bar{\Lambda}$ (red) and $\Sigma^-\bar{\Lambda}$ pair (blue) production in ^{136}Xe vs. ^{129}Xe nuclei as a function of the impact parameter.

parameter set. The same parametrization also enters during the time evolution of the reaction. Of course, any interpretation of experimental data should be constrained to simulations, which describe the proton distributions (and other possible observables) reasonably well. In the following we use three RMF descriptions, the NL1 [57], NL3, and NL3* [60], which provide slightly different proton and neutron distributions. In all three cases the proton radii are close to the experimental values (see Table I). In line with the similar proton and neutron distributions, the double ratios from the GiBUU simulations agree within statistical uncertainties for all three cases (see Table II).

V. SENSITIVITY OF THE METHOD

The results for the xenon isotopes give some hint for the sensitivity of the double ratio to the thickness of the neutron skin. It is however desirable to determine the sensitivity of the double ratio to the neutron skin variation more quantitatively. In the GiBUU model, the initial density distributions are generated with the same interaction model which is used in the transport stage. It is, therefore, not possible to use density distributions with different neutron skins in the same transport simulation.

In Figure 8 we depict the double ratio deduced from the neutron-proton content of the nuclear periphery as described in section III as a function of the double ratio predicted by the GiBUU transport calculations of 2.4 GeV/c \bar{p} +A interactions. The systematic difference between the two double ratios can be at least in part traced back to the differences in absorption of antihyperons and hyperons, which is particularly large

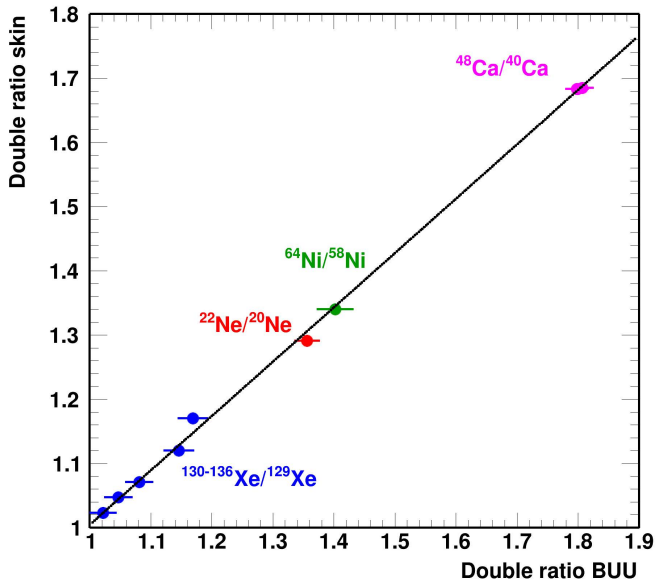


FIG. 8. Double ratio deduced from the neutron-proton content of the nuclear periphery as described in section III as a function of the double ratio predicted by the GiBUU transport calculations of 2.4 GeV/c \bar{p} +A interactions. The black line is a linear fit to the data.

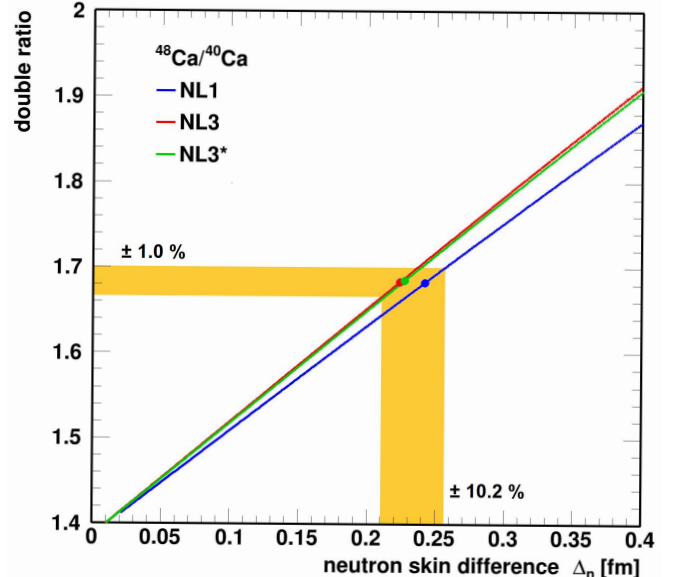


FIG. 9. Double ratio deduced from the neutron-proton content of the nuclear periphery versus the difference of the neutron skin thickness Δ_n for ^{40}Ca and ^{48}Ca . In order to explore the effect of different neutron skins for ^{48}Ca , its neutron distribution generated by GiBUU was artificially compressed by a given factor, while the proton distribution and the distributions for ^{40}Ca remained unchanged. The density distributions are generated during the initialization of the GiBUU simulations [62] using the RMF parameter set of Ref. [57].

at small impact parameters, where the double ratio is smaller (cf. Figure 7 and Figure 3). In our simple schematic model this effect has been neglected. Nonetheless, the strong correlation between the two quantities suggests that our simple model accounts for the main features of the reaction process. Thus, the schematic model of section III allows to explore the sensitivity of the method by tuning the neutron distributions of one nucleus without changing the neutron distribution of the reference nucleus and the proton distributions.

In the following we concentrate on the combination of ^{40}Ca and ^{48}Ca . As before, the density distributions are generated with the initialization code of the GiBUU simulations [62] using different RMF parameter sets of Ref. [57]. We consider here only parameter sets which give a reasonable value for the proton radii. To modify the neutron skin thickness, we radially squeezed resp. stretched the neutron distribution of ^{48}Ca by scaling the half-density radius. The density was changed accordingly to keep the number of neutrons the same. The ^{40}Ca nucleus remained unchanged. Figure 9 shows the double ratio calculated as described in section III versus the difference Δ_n of the neutron skin difference between the ^{40}Ca and the modified ^{48}Ca nucleus, $\Delta_n = \Delta R_{pn}(^{48}\text{Ca}) - \Delta R_{pn}(^{40}\text{Ca})$. The symbols on each line mark the double ratio and neutron skin difference for the original density distributions (c.f. Table I). For all three interaction parameters we find a very similar linear relation between the double ratio and Δ_n . Including possible systematic variations due to different interactions, an uncertainty of the double ratio of $\pm 1\%$, which is typical for the present work (see Table II) translates into an uncertainty of

the neutron skin variation by about $\pm 10\%$ (see yellow bands in Figure 9). This is about a factor of three smaller compared to the uncertainty of the CREX result.

Of course, the study of possible model dependencies can not only rely on measured double ratios. Additional observables or reaction parameters like the absolute cross sections, the angular distributions or co-planarity of the produced hyperon-antihyperon pairs can help to constrain the transport calculations and may help to reduce systematic uncertainties. Statistical uncertainties can easily be reduced by longer measurement periods (see below).

In the present work we focused on an incident antiproton of $2.4 \text{ GeV}/c$. Of course, the beam momentum needs to be optimized with respect to e.g. the production yields, experimental efficiency and sensitivity. In particular, the $\Sigma^-\bar{\Lambda}$ pair production will be reduced at lower beam momenta. Preliminary results for the neon case at a lower momentum of $1.7 \text{ GeV}/c$ have been presented earlier [72]. Due to the larger $\bar{p}+n$ cross section of 63 mb at an antiproton momentum $1.7 \text{ GeV}/c$, the schematic model of section III predicts an increase of the double ratio by about 1.4% as compared to the case of $2.4 \text{ GeV}/c$. The GiBUU simulations (with improved statistics as presented in [72]) predict a double ration of 1.440 ± 0.054 and hence a somewhat larger increase by $6.2 \pm 4.1\%$. However, the statistical uncertainty is still rather large due to the limited computing time. Though this explorative result suggests that the incident antiproton momentum has only a small effect on the double ratio, a systematic study with larger event samples is clearly desirable.

VI. EXPERIMENTAL ASPECTS AND OUTLOOK

The proposed method focuses on the total production ratios of $\Lambda\bar{\Lambda}$ and $\Sigma^-\bar{\Lambda}$ pairs. While the masses of the Λ and $\bar{\Lambda}$ hyperons can be easily identified by the charged decay channel, the reconstruction of the $\Sigma^- \rightarrow \pi^+ n$ decay will be complicated by the required neutron detection. The reduced Σ^- mass resolution will of course increase the background for $\Sigma^-\bar{\Lambda}$ pairs. Nevertheless, in the double ratio, many systematic effects will cancel. Furthermore, $\bar{p}-p$ and $\bar{p}-d$ interactions will provide important points of reference. At $\bar{\text{P}}\text{ANDA}$ a reconstruction efficiency of 30% , 30% , and 2% is expected for Λ , $\bar{\Lambda}$, and Σ^- , respectively [73]. Even with a moderate average interaction rate of $2 \cdot 10^6 \text{ s}^{-1}$, the statistical precision shown in Table II e.g. for calcium can be reached in about half a day running for each isotope. Although the additional background particularly for the Σ^- may require somewhat larger measuring periods, this estimate demonstrates the large potential of this method for a precision study at an antiproton storage ring.

With the regular pellet target system of the $\bar{\text{P}}\text{ANDA}$ setup, all noble gases can be employed. But even with a cleaning and recirculation system the operation of such isotopically enriched gaseous isotopes will be rather costly. Instead, with a filament target system similar to the one, which has been developed for the hyperatom studies at $\bar{\text{P}}\text{ANDA}$ [74, 75], also many solid nuclear targets are also feasible. Note, that only

a few milligrams of material is needed for such a target filaments. While we have focused in this work on the two double magic calcium isotopes, also additional calcium isotopes or many other isotope chains like e.g. $^{58-64}\text{Ni}$ [76] will therefore be experimentally accessible at a reasonably price, enrichment [77] and measuring time. For specific Isotope pairs, where sufficient target material is available, also a measurement in a fixed target mode may be feasible, e.g. making use of the antiproton beam at J-PARC [78].

Finally we note, that an analogous method might also allow to explore the evolution of the proton skin thickness in isotope chains. Combined with precise data on the proton distributions this might give access to the neutron distributions in proton rich isotones.

ACKNOWLEDGMENTS

We are grateful to Patrick Achenbach for supporting discussions during the early stage of this work. This project has received funding from the European Union's Horizon 2020 research and innovation programme under grant agreement No 824093. The presented data were collected within the framework of the PhD thesis of Falk Schupp [73] and in part within the bachelor thesis of Martin Christiansen [79, 80] at the Johannes Gutenberg University Mainz. Calculations for this project were performed on the HPC cluster "HIMster2" at the Helmholtz Institute Mainz. "HIMster2" is a part of Mogon2 and we thank the HPC department of the Johannes Gutenberg University Mainz [81] for their efforts in maintaining the cluster.

F.S. performed the calculations and the analysis. He was responsible for the visualization of the published work and he also took part in the preparation, the review, and the editing of the manuscript. J.P. conceptualized the work, supervised the work and prepared the original draft. M.B. M.C. and M.S. contributed to the data visualization and data collection, T.G. and H.L. helped in implementing the computer code and validation of the results. They also took part in the review and editing process.

Appendix

The following tables Table III and Table IV collect the values and references displayed in Figure 1.

Method	Ref.	R_p [fm]	R_n [fm]	ΔR_{pn} [fm]
10.8-16.3 MeV p elastic scattering	[82]	3.38	3.78 ± 0.09	0.39 ± 0.10
166 MeV α elastic scattering	[83]	3.39	3.72 ± 0.12	0.33 ± 0.12
1044 MeV p elastic scattering	[13]	3.48	3.66	0.16 ± 0.023
1370 MeV α elastic scattering	[84]	3.48	3.67 ± 0.05	0.19 ± 0.05
π^- and π^+ scattering	[85]			0.20 ± 0.09^1
1040 MeV p elastic scattering	[86]	3.38	3.54	0.16 ± 0.05
104 MeV α elastic scattering	[87]			0.17 ± 0.10
1040 MeV p scattering	[26]	3.41	$3.58 \pm 0.04 \pm 0.1$	$0.18 \pm 0.04 \pm 0.1$
800 MeV $\vec{p} + {}^{48}\text{Ca}$	[88]	3.376^1	3.561^1	0.18 ± 0.08
π^- and π^+ scattering	[14, 15]	3.32 ± 0.03	3.43 ± 0.03	0.11 ± 0.04
analysis of antiprotonic atoms	[16]			$0.12^{+0.04}_{-0.08}$
500-1040 MeV p scattering	[28]		3.436 ± 0.023	0.079 ± 0.023
electric dipole polarizability	[41]			0.17 ± 0.03
$n + {}^{48}\text{Ca}$ and $p + {}^{48}\text{Ca}$ scattering	[89]			0.249 ± 0.023
${}^{48}\text{Ca} + {}^{12}\text{C}$ interaction cross section	[32]			0.197 ± 0.048
$p + {}^{48}\text{Ca}$ and ${}^{48}\text{Ca} + {}^{12}\text{C}$ scattering	[21]			$0.158 \pm 0.023(\text{exp}) \pm 0.012(\text{mod})$
$p + {}^{48}\text{Ca}$ and ${}^{48}\text{Ca} + {}^{12}\text{C}$ scattering	[33]		3.43 ± 0.16	
CREX	[25]			$0.121 \pm 0.026(\text{exp}) \pm 0.024(\text{mod})$

¹assuming $R_p=R_n$ for ${}^{40}\text{Ca}$.

TABLE III. Published radii of protons and neutrons in ${}^{48}\text{Ca}$ which are shown in Figure 1.

Method	Ref.	$R_{\text{rms}}(n)$ - $R_{\text{rms}}(p)$ [fm]	remark
elastic p and n scattering at 40, 65, 200 MeV	[27]	0.17	
elastic p scattering at 295 MeV	[18]	$0.211^{+0.054}_{-0.063}$	
elastic p scattering at 650 MeV	[90, 91]	0.20 ± 0.04	
$p + {}^{208}\text{Pb}$ reaction cross section at 30 - 100 MeV	[31]	0.278 ± 0.035	
${}^{208}\text{Pb} + {}^{208}\text{Pb}$ at LHC	[34]	0.217 ± 0.058	
antiprotonic atoms	[92]	$0.16 \pm (0.02)_{\text{stat}} \pm (0.04)_{\text{syst}}$	
	[93]	0.21 ± 0.03	
	[94]	$0.20 \pm (0.04)_{\text{exp}} \pm (0.04)_{\text{theo}}$	reanalysis of [92]
strength of pigmy dipole resonance	[95]	0.18 ± 0.035	
	[38]	0.194 ± 0.024	
electric dipole polarizability	[40]	$0.156^{+0.025}_{-0.021}$	
by \vec{p} -scattering at 295 MeV	[96]	$0.165 \pm (0.009)_{\text{exp}} \pm (0.013)_{\text{theo}} \pm (0.021)_{\text{est}}$	
	[40, 97]	0.168 ± 0.022	reanalysis of [40]
giant dipole resonance; 120 MeV α -scattering	[36]	0.19 ± 0.09	see [37]
giant dipole resonance; 196 MeV α -scattering	[37, 98]	0.12 ± 0.07	
anti-analog giant dipole resonance	[99]	0.161 ± 0.042	
	[100, 101]	$0.216 \pm (0.046)_{\text{exp}} \pm (0.015)_{\text{theo}}$	
coherent π^0 production	[42]	0.15 ± 0.03 (stat.) $^{+0.01}_{-0.03}$ (sys.)	
parity violating e^- scattering	[23]	$0.33^{+0.16}_{-0.18}$	
parity violating e^- scattering PREX 1+2	[24]	0.283 ± 0.071	
tidal deformability from neutron star merger	[44]	≤ 0.25	analysis of [45]
NICER	[102, 103]	≤ 0.31	analysis of [46]

TABLE IV. The neutron skin thickness $\Delta R_{np} = R_{\text{rms}}(n) - R_{\text{rms}}(p)$ of ${}^{208}\text{Pb}$ deduced by different experiments and analyses as shown in Figure 1.

- [1] M. B. Tsang, J. R. Stone, F. Camera, P. Danielewicz, S. Gandolfi, K. Hebeler, C. J. Horowitz, J. Lee, W. G. Lynch, Z. Kohley, R. Lemmon, P. Möller, T. Murakami, S. Riordan, X. Rocamaza, F. Sammarruca, A. W. Steiner, I. Vidaña, and S. J. Yennello, Constraints on the symmetry energy and neutron skins from experiments and theory, Phys. Rev. C **86**, 015803 (2012).

- [2] M. Baldo and G. Burgio, The nuclear symmetry energy, Progress in Particle and Nuclear Physics **91**, 203 (2016).
[3] J. Piekarewicz and F. J. Fattoyev, Neutron-rich matter in heaven and on earth, Physics Today **72**, 30 (2019), <https://doi.org/10.1063/PT.3.4247>.

- [4] B. Alex Brown, Neutron radii in nuclei and the neutron equation of state, Phys. Rev. Lett. **85**, 5296 (2000).
- [5] C. J. Horowitz and J. Piekarewicz, Neutron Star Structure and the Neutron Radius of ^{208}Pb , Phys. Rev. Lett. **86**, 5647 (2001).
- [6] S. Typel and B. A. Brown, Neutron radii and the neutron equation of state in relativistic models, Phys. Rev. C **64**, 027302 (2001).
- [7] C. J. Horowitz and J. Piekarewicz, Neutron radii of ^{208}Pb and neutron stars, Phys. Rev. C **64**, 062802 (2001).
- [8] F. Sammarruca and P. Liu, Neutron skin of ^{208}Pb and density dependence of the symmetry energy, Phys. Rev. C **79**, 057301 (2009).
- [9] X. Roca-Maza, M. Brenna, B. K. Agrawal, P. F. Bortignon, G. Colo, L.-G. Cao, N. Paar, and D. Vretenar, Giant quadrupole resonances in ^{208}Pb , the nuclear symmetry energy, and the neutron skin thickness, Phys. Rev. C **87**, 034301 (2013).
- [10] P.-G. Reinhard and W. Nazarewicz, Nuclear charge and neutron radii and nuclear matter: Trend analysis in skyrme density-functional-theory approach, Phys. Rev. C **93**, 051303 (2016).
- [11] M. Centelles, X. Roca-Maza, X. Viñas, and M. Warda, Nuclear symmetry energy probed by neutron skin thickness of nuclei, Phys. Rev. Lett. **102**, 122502 (2009).
- [12] T. Suzuki, H. Geissel, O. Bochkarev, L. Chulkov, M. Golovkov, D. Hirata, H. Irnich, Z. Janas, H. Keller, T. Kobayashi, G. Kraus, G. Münzenberg, S. Neumaier, F. Nickel, A. Ozawa, A. Piechaczeck, E. Roeckl, W. Schwab, K. Sümerer, K. Yoshida, and I. Tanihata, Neutron skin of na isotopes studied via their interaction cross sections, Phys. Rev. Lett. **75**, 3241 (1995).
- [13] G. Alkhazov, T. Bauer, R. Beurtey, A. Boudard, G. Bruge, A. Chaumeaux, P. Couvert, G. Cvijanovich, H. Duhm, J. Fontaine, D. Garreta, A. Kulikov, D. Legrand, J. Lugol, J. Saudinos, J. Thirion, and A. Vorobyov, Elastic and inelastic scattering of 1.044 GeV protons by ^{40}Ca , ^{42}Ca , ^{44}Ca , ^{48}Ca and ^{48}Ti , Nuclear Physics A **274**, 443 (1976).
- [14] K. G. Boyer, W. J. Braithwaite, W. B. Cottingham, S. J. Greene, L. E. Smith, C. F. Moore, C. L. Morris, H. A. Thiessen, G. S. Blanpied, G. R. Burleson, J. F. Davis, J. S. McCarthy, R. C. Minehart, and C. A. Goulding, Pion elastic and inelastic scattering from $^{40,42,44,48}\text{Ca}$ and ^{54}Fe , Phys. Rev. C **29**, 182 (1984).
- [15] W. R. Gibbs and J.-P. Dedonder, Neutron radii of the calcium isotopes, Phys. Rev. C **46**, 1825 (1992).
- [16] F. J. Hartmann, R. Schmidt, B. Ketzer, T. von Egidy, S. Wycech, R. Smolańczuk, T. Czosnyka, J. Jastrzębski, M. Kisielinski, P. Lubiński, P. Napiorkowski, L. Pieńkowski, A. Trzcińska, B. Kłos, K. Gulda, W. Kurcewicz, and E. Widmann, Nucleon density in the nuclear periphery determined with antiprotonic x rays: Calcium isotopes, Phys. Rev. C **65**, 014306 (2001).
- [17] T. Yamaguchi, T. Suzuki, T. Ohnishi, F. Becker, M. Fukuda, H. Geissel, M. Hosoi, R. Janik, K. Kimura, T. Kuboki, S. Mandel, M. Matsuo, G. Münzenberg, S. Nakajima, T. Ohtsubo, A. Ozawa, A. Prochazka, M. Shindo, B. Sitár, P. Strmeň, T. Suda, K. Sümerer, K. Sugawara, I. Szarka, M. Takechi, A. Takisawa, K. Tanaka, and M. Yamagami, Nuclear matter radii of neutron-deficient kr isotopes, Phys. Rev. C **77**, 034315 (2008).
- [18] J. Zenihiro, H. Sakaguchi, T. Murakami, M. Yosoi, Y. Yasuda, S. Terashima, Y. Iwao, H. Takeda, M. Itoh, H. P. Yoshida, and M. Uchida, Neutron density distributions of $^{204,206,208}\text{Pb}$ deduced via proton elastic scattering at $E_p = 295$ MeV, Phys. Rev. C **82**, 044611 (2010).
- [19] S. Mizutori, J. Dobaczewski, G. A. Lalazissis, W. Nazarewicz, and P.-G. Reinhard, Nuclear skins and halos in the mean-field theory, Phys. Rev. C **61**, 044326 (2000).
- [20] C. Horowitz, K. Kumar, and R. Michaels, Electroweak measurements of neutron densities in CREX and PREX at JLab, USA, The European Physical Journal A **50**, 48 (2014).
- [21] S. Tagami, T. Wakasa, M. Takechi, J. Matsui, and M. Yahiro, Neutron skin in ^{48}Ca determined from $\text{p} + ^{48}\text{Ca}$ and $^{48}\text{Ca} + ^{12}\text{C}$ scattering, Results in Physics **33**, 105155 (2022).
- [22] C. H. Hyun, Neutron Skin Thickness of ^{48}Ca , ^{132}Sn , and ^{208}Pb with KIDS Density Functional, The origin of New Physics: Sae Mulli **72**, 371 (2022).
- [23] S. Abrahamyan, Z. Ahmed, H. Albataineh, K. Aniol, D. S. Armstrong, W. Armstrong, T. Averett, B. Babineau, A. Barberi, V. Bellini, R. Beminiwattha, J. Benesch, F. Benmokhtar, T. Bielański, W. Boeglin, A. Camsonne, M. Canan, P. Carter, G. D. Cates, C. Chen, J.-P. Chen, O. Hen, F. Cusanno, M. M. Dalton, R. De Leo, K. de Jager, W. Deconinck, P. Decowski, X. Deng, A. Deur, D. Dutta, A. Etile, D. Flay, G. B. Franklin, M. Friend, S. Frullani, E. Fuchey, F. Garibaldi, E. Gasser, R. Gilman, A. Giusa, A. Glamazdin, J. Gomez, J. Grames, C. Gu, O. Hansen, J. Hansknecht, D. W. Higinbotham, R. S. Holmes, T. Holmstrom, C. J. Horowitz, J. Hoskins, J. Huang, C. E. Hyde, F. Itard, C.-M. Jen, E. Jensen, G. Jin, S. Johnston, A. Kelleher, K. Kliakhandler, P. M. King, S. Kowalski, K. S. Kumar, J. Leacock, J. Leckey, J. H. Lee, J. J. LeRose, R. Lindgren, N. Liyanage, N. Lubinsky, J. Mammei, F. Mammoliti, D. J. Margaziotis, P. Markowitz, A. McCreary, D. McNulty, L. Mercado, Z.-E. Meziani, R. W. Michaels, M. Mihovilovic, N. Muangma, C. Muñoz Camacho, S. Nanda, V. Nelyubin, N. Nuruzzaman, Y. Oh, A. Palmer, D. Parno, K. D. Paschke, S. K. Phillips, B. Poelker, R. Pomatsalyuk, M. Posik, A. J. R. Puckett, B. Quinn, A. Rakhman, P. E. Reimer, S. Riordan, P. Rogan, G. Ron, G. Russo, K. Saenboonruang, A. Saha, B. Sawatzky, A. Shahinyan, R. Silwal, S. Sirca, K. Slifer, P. Solvignon, P. A. Souder, M. L. Sperduto, R. Subedi, R. Suleiman, V. Sulcosky, C. M. Sutera, W. A. Tobias, W. Troth, G. M. Urciuoli, B. Waidyawansa, D. Wang, J. Wexler, R. Wilson, B. Wojtsekhowski, X. Yan, H. Yao, Y. Ye, Z. Ye, V. Yim, L. Zana, X. Zhan, J. Zhang, Y. Zhang, X. Zheng, and P. Zhu (PREX Collaboration), Measurement of the neutron radius of ^{208}Pb through parity violation in electron scattering, Phys. Rev. Lett. **108**, 112502 (2012).
- [24] D. Adhikari, H. Albataineh, D. Androic, K. Aniol, D. S. Armstrong, T. Averett, C. Ayerbe Gayoso, S. Barcus, V. Bellini, R. S. Beminiwattha, J. F. Benesch, H. Bhatt, D. Bhatta Pathak, D. Bhetuwal, B. Blaikie, Q. Campagna, A. Camsonne, G. D. Cates, Y. Chen, C. Clarke, J. C. Cornejo, S. Covrig Dusa, P. Datta, A. Deshpande, D. Dutta, C. Feldman, E. Fuchey, C. Gal, D. Gaskell, T. Gautam, M. Gericke, C. Ghosh, I. Halilovic, J.-O. Hansen, F. Hauenstein, W. Henry, C. J. Horowitz, C. Jantzi, S. Jian, S. Johnston, D. C. Jones, B. Karki, S. Katugampola, C. Keppel, P. M. King, D. E. King, M. Knauss, K. S. Kumar, T. Kutz, N. Lashley-Colthirst, G. Leverick, H. Liu, N. Liyange, S. Malace, R. Mammei, J. Mammei, M. McCaughan, D. McNulty, D. Meekins, C. Metts, R. Michaels, M. M. Mondal, J. Napolitano, A. Narayan, D. Nikolaev, M. N. H. Rashad, V. Owen, C. Palatchi, J. Pan, B. Pandey, S. Park, K. D. Paschke, M. Petrusky, M. L. Pitt, S. Premathilake, A. J. R. Puckett, B. Quinn, R. Radloff, S. Rahman, A. Rathnayake, B. T. Reed, P. E. Reimer, R. Richards, S. Riordan, Y. Roblin, S. Seeds,

- A. Shahinyan, P. Souder, L. Tang, M. Thiel, Y. Tian, G. M. Urciuoli, E. W. Wertz, B. Wojtsekowski, B. Yale, T. Ye, A. Yoon, A. Zec, W. Zhang, J. Zhang, and X. Zheng (PREX Collaboration), Accurate determination of the neutron skin thickness of ^{208}Pb through parity-violation in electron scattering, *Phys. Rev. Lett.* **126**, 172502 (2021).
- [25] D. Adhikari, H. Albataineh, D. Androic, K. A. Aniol, D. S. Armstrong, T. Averett, C. Ayerbe Gayoso, S. K. Barcus, V. Bellini, R. S. Beminiwattha, J. F. Benesch, H. Bhatt, D. Bhatta Pathak, D. Bhetuwal, B. Blaikie, J. Boyd, Q. Campagna, A. Camsonne, G. D. Cates, Y. Chen, C. Clarke, J. C. Cornejo, S. Covrig Dusa, M. M. Dalton, P. Datta, A. Deshpande, D. Dutta, C. Feldman, E. Fuchey, C. Gal, D. Gaskell, T. Gautam, M. Gericke, C. Ghosh, I. Halilovic, J.-O. Hansen, O. Hassan, F. Hauenstein, W. Henry, C. J. Horowitz, C. Jantzi, S. Jian, S. Johnston, D. C. Jones, S. Kakkar, S. Katugampola, C. Keppel, P. M. King, D. E. King, K. S. Kumar, T. Kutz, N. Lashley-Colthirst, G. Leverick, H. Liu, N. Liyanage, J. Mammei, R. Mammei, M. McCaughan, D. McNulty, D. Meekins, C. Metts, R. Michaels, M. Mihovilovic, M. M. Mondal, J. Napolitano, A. Narayan, D. Nikolaev, V. Owen, C. Palatchi, J. Pan, B. Pandey, S. Park, K. D. Paschke, M. Petrusky, M. L. Pitt, S. Premathilake, B. Quinn, R. Radloff, S. Rahman, M. N. H. Rashad, A. Rathnayake, B. T. Reed, P. E. Reimer, R. Richards, S. Riordan, Y. R. Roblin, S. Seeds, A. Shahinyan, P. Souder, M. Thiel, Y. Tian, G. M. Urciuoli, E. W. Wertz, B. Wojtsekowski, B. Yale, T. Ye, A. Yoon, W. Xiong, A. Zec, W. Zhang, J. Zhang, and X. Zheng (CREX Collaboration), Precision determination of the neutral weak form factor of ^{48}Ca , *Phys. Rev. Lett.* **129**, 042501 (2022).
- [26] I. Brissaud and X. Campi, Determination of matter densities of Ca isotopes by 600 MeV and 1 GeV proton elastic scattering, *Physics Letters B* **86**, 141 (1979).
- [27] S. Karataglidis, K. Amos, B. Brown, and P. Deb, Discerning the neutron density distribution of ^{208}Pb from nucleon elastic scattering, *Phys. Rev. C* **65**, 044306 (2002).
- [28] B. C. Clark, L. J. Kerr, and S. Hama, Neutron densities from a global analysis of medium-energy proton-nucleus elastic scattering, *Phys. Rev. C* **67**, 054605 (2003).
- [29] H. Sakaguchi and J. Zenihiro, Proton elastic scattering from stable and unstable nuclei - extraction of nuclear densities, *Progress in Particle and Nuclear Physics* **97**, 1 (2017).
- [30] I. A. M. Abdul-Magead, E. Hamza, and B. Abu-Ibrahim, Neutron radii and neutron skin of neutron-rich nuclei deduced from proton-nucleus total reaction cross sections, *Journal of Physics G: Nuclear and Particle Physics* **47**, 055103 (2020).
- [31] S. Tagami, T. Wakasa, J. Matsui, M. Yahiro, and M. Takechi, Neutron skin thickness of ^{208}Pb determined from the reaction cross section for proton scattering, *Phys. Rev. C* **104**, 024606 (2021).
- [32] M. Tanaka, M. Takechi, A. Homma, M. Fukuda, D. Nishimura, T. Suzuki, Y. Tanaka, T. Moriguchi, D. S. Ahn, A. Aimaganbetov, M. Amano, H. Arakawa, S. Bagchi, K.-H. Behr, N. Burtebayev, K. Chikaato, H. Du, S. Ebata, T. Fujii, N. Fukuda, H. Geissel, T. Hori, W. Horiuchi, S. Hoshino, R. Igosawa, A. Ikeda, N. Inabe, K. Inomata, K. Itahashi, T. Izumikawa, D. Kamioka, N. Kanda, I. Kato, I. Kenzhina, Z. Korkulu, Y. Kuk, K. Kusaka, K. Matsuta, M. Miura, E. Miyata, D. Nagae, S. Nakamura, M. Nasurilla, K. Nishimuro, K. Nishizuka, K. Ohnishi, M. Ohtake, T. Ohtsubo, S. Omika, H. J. Ong, A. Ozawa, A. Prochazka, H. Sakurai, C. Scheidenberger, Y. Shimizu, T. Sugihara, T. Sumikama, H. Suzuki, S. Suzuki, H. Takeda, Y. K. Tanaka, I. Tanihata, T. Wada, K. Wakayama, S. Yagi, T. Yamaguchi, R. Yanagihara, Y. Yanagisawa, K. Yoshida, and T. K. Zholdybayev, Swelling of Doubly Magic ^{48}Ca Core in Ca Isotopes beyond $N = 28$, *Phys. Rev. Lett.* **124**, 102501 (2020).
- [33] I. A. M. Abdul-Magead and B. Abu-Ibrahim, Neutron skin of neutron-rich nuclei, *Phys. Rev. C* **105**, 014626 (2022).
- [34] G. Giacalone, G. Nijs, and W. van der Schee, Determination of the neutron skin of ^{208}Pb from ultrarelativistic nuclear collisions, *Phys. Rev. Lett.* **131**, 202302 (2023).
- [35] H. Lenske and P. Kienle, Probing matter radii of neutron-rich nuclei by antiproton scattering, *Physics Letters B* **647**, 82 (2007).
- [36] A. Krasznahorkay, J. Bacelar, J. A. Bordewijk, S. Brandenburg, A. Buda, G. van 't Hof, M. A. Hofstee, S. Kato, T. D. Poelhekken, S. Y. van der Werf, A. van der Woude, M. N. Harakeh, and N. Kalantar-Nayestanaki, Excitation of the isovector giant dipole resonance by inelastic α scattering and the neutron skin of nuclei, *Phys. Rev. Lett.* **66**, 1287 (1991).
- [37] A. Krasznahorkay, H. Akimune, A. van den Berg, N. Blasi, S. Brandenburg, M. Csatlós, M. Fujiwara, J. Gulyás, M. Harakeh, M. Hunyadi, M. de Huu, Z. Mate, D. Sohler, S. van der Werf, H. Wörtche, and L. Zolnai, Neutron-skin thickness in neutron-rich isotopes, *Nuclear Physics A* **731**, 224 (2004).
- [38] A. Carbone, G. Colò, A. Bracco, L.-G. Cao, P. F. Bortignon, F. Camera, and O. Wieland, Constraints on the symmetry energy and neutron skins from pygmy resonances in ^{68}Ni and ^{132}Sn , *Phys. Rev. C* **81**, 041301 (2010).
- [39] A. Krasznahorkay, M. Fujiwara, P. van Aarle, H. Akimune, I. Daito, H. Fujimura, Y. Fujita, M. N. Harakeh, T. Inomata, J. Jänecke, S. Nakayama, A. Tamii, M. Tanaka, H. Toyokawa, W. Uijen, and M. Yosoi, Excitation of isovector spin-dipole resonances and neutron skin of nuclei, *Phys. Rev. Lett.* **82**, 3216 (1999).
- [40] A. Tamii, I. Poltoratska, P. von Neumann-Cosel, Y. Fujita, T. Adachi, C. A. Bertulani, J. Carter, M. Dozono, H. Fujita, K. Fujita, K. Hatanaka, D. Ishikawa, M. Itoh, T. Kawabata, Y. Kalmykov, A. M. Krumbholz, E. Litvinova, H. Matsubara, K. Nakanishi, R. Neveling, H. Okamura, H. J. Ong, B. Özeltashenov, V. Y. Ponomarev, A. Richter, B. Rubio, H. Sakaguchi, Y. Sakemi, Y. Sasamoto, Y. Shimbara, Y. Shimizu, F. D. Smit, T. Suzuki, Y. Tameshige, J. Wambach, R. Yamada, M. Yosoi, and J. Zenihiro, Complete Electric Dipole Response and the Neutron Skin in ^{208}Pb , *Phys. Rev. Lett.* **107**, 062502 (2011).
- [41] J. Birkhan, M. Miorelli, S. Bacca, S. Bassauer, C. A. Bertulani, G. Hagen, H. Matsubara, P. von Neumann-Cosel, T. Papenbrock, N. Pietralla, V. Y. Ponomarev, A. Richter, A. Schwenk, and A. Tamii, Electric dipole polarizability of ^{48}Ca and implications for the neutron skin, *Phys. Rev. Lett.* **118**, 252501 (2017).
- [42] C. M. Tarbert, D. P. Watts, D. I. Glazier, P. Aguilar, J. Ahrens, J. R. M. Annand, H. J. Arends, R. Beck, V. Bekrenev, B. Boillat, A. Braghieri, D. Branford, W. J. Briscoe, J. Brudvik, S. Cherepyna, R. Codling, E. J. Downie, K. Foehl, P. Grabmayr, R. Gregor, E. Heid, D. Hornidge, O. Jahn, V. L. Kashevvarov, A. Knezevic, R. Kondratiev, M. Korolija, M. Kotulla, D. Krambrich, B. Krusche, M. Lang, V. Lisin, K. Livingston, S. Lugert, I. J. D. MacGregor, D. M. Manley, M. Martinez, J. C. McGeorge, D. Mekterovic, V. Metag, B. M. K. Nefkens, A. Nikolaev, R. Novotny, R. O. Owens, P. Pedroni, A. Polonski, S. N. Prakhov, J. W. Price, G. Rosner, M. Rost, T. Rostomyan, S. Schadmand, S. Schumann, D. Sober, A. Starostin, I. Supek, A. Thomas, M. Unverzagt, T. Walcher, L. Zana, and

- F. Zehr (Crystal Ball at MAMI and A2 Collaboration), Neutron skin of ^{208}Pb from coherent pion photoproduction, *Phys. Rev. Lett.* **112**, 242502 (2014).
- [43] A. Trzcińska, J. Jastrzębski, P. Lubiński, F. Hartmann, R. Schmidt, T. von Egidy, and B. Kłos, Neutron density distributions deduced from antiprotonic atoms, *Phys. Rev. Lett.* **87**, 082501 (2001).
- [44] F. J. Fattoyev, J. Piekarewicz, and C. J. Horowitz, Neutron skins and neutron stars in the multimessenger era, *Phys. Rev. Lett.* **120**, 172702 (2018).
- [45] B. Abbott, R. Abbott, T. D. Abbott, F. Acernese, K. Ackley, C. Adams, T. Adams, P. Addesso, R. X. Adhikari, V. B. Adya, C. Affeldt, M. Afrough, B. Agarwal, M. Agathos, K. Agatsuma, *et al.* (LIGO Scientific Collaboration and Virgo Collaboration), Gw170817: Observation of gravitational waves from a binary neutron star inspiral, *Phys. Rev. Lett.* **119**, 161101 (2017).
- [46] B. T. Reed, F. J. Fattoyev, C. J. Horowitz, and J. Piekarewicz, Implications of prex-2 on the equation of state of neutron-rich matter, *Phys. Rev. Lett.* **126**, 172503 (2021).
- [47] G. A. Miller, Coherent-nuclear pion photoproduction and neutron radii, *Phys. Rev. C* **100**, 044608 (2019).
- [48] A. Ekström, G. R. Jansen, K. A. Wendt, G. Hagen, T. Papenbrock, B. D. Carlsson, C. Forssén, M. Hjorth-Jensen, P. Navrátil, and W. Nazarewicz, Accurate nuclear radii and binding energies from a chiral interaction, *Phys. Rev. C* **91**, 051301 (2015).
- [49] J. E. Sobczyk, B. Acharya, S. Bacca, and G. Hagen, Ab initio computation of the longitudinal response function in ^{40}Ca , *Phys. Rev. Lett.* **127**, 072501 (2021).
- [50] K. Hebeler, Three-nucleon forces: Implementation and applications to atomic nuclei and dense matter, *Physics Reports* **890**, 1 (2021), three-nucleon forces: Implementation and applications to atomic nuclei and dense matter.
- [51] C. McIlroy, C. Barbieri, T. Inoue, T. Doi, and T. Hatsuda, Doubly magic nuclei from lattice qcd forces at $M_{\text{ps}} = 469 \text{ MeV}/c^2$, *Phys. Rev. C* **97**, 021303 (2018).
- [52] T. Miyagi, T. Abe, M. Kohno, P. Navrátil, R. Okamoto, T. Otsuka, N. Shimizu, and S. R. Stroberg, Ground-state properties of doubly magic nuclei from the unitary-model-operator approach with chiral two- and three-nucleon forces, *Phys. Rev. C* **100**, 034310 (2019).
- [53] M. C. Atkinson, M. H. Mahzoon, M. A. Keim, B. A. Bordelon, C. D. Pruitt, R. J. Charity, and W. H. Dickhoff, Dispersive optical model analysis of ^{208}Pb generating a neutron-skin prediction beyond the mean field, *Phys. Rev. C* **101**, 044303 (2020).
- [54] C. D. Pruitt, R. J. Charity, L. G. Sobotka, M. C. Atkinson, and W. H. Dickhoff, Systematic matter and binding-energy distributions from a dispersive optical model analysis, *Phys. Rev. Lett.* **125**, 102501 (2020).
- [55] P.-G. Reinhard, X. Roca-Maza, and W. Nazarewicz, Combined theoretical analysis of the parity-violating asymmetry for ^{48}Ca and ^{208}Pb , *Phys. Rev. Lett.* **129**, 232501 (2022).
- [56] H. D. Vries, C. D. Jager, and C. D. Vries, Nuclear charge-density-distribution parameters from elastic electron scattering, *Atomic Data and Nuclear Data Tables* **36**, 495 (1987).
- [57] G. A. Lalazissis, J. König, and P. Ring, New parametrization for the lagrangian density of relativistic mean field theory, *Phys. Rev. C* **55**, 540 (1997).
- [58] I. Angeli and K. Marinova, Table of experimental nuclear ground state charge radii: An update, *Atomic Data and Nuclear Data Tables* **99**, 69 (2013).
- [59] R. F. Garcia Ruiz, M. L. Bissell, K. Blaum, A. Ekström, N. Frömmgen, G. Hagen, M. Hammen, K. Hebeler, J. D. Holt, G. R. Jansen, M. Kowalska, K. Kreim, W. Nazarewicz, R. Neugart, G. Neyens, W. Nörterhäuser, T. Papenbrock, J. Papuga, A. Schwenk, J. Simonis, K. Wendt, and D. T. Yordanov, Unexpectedly large charge radii of neutron-rich calcium isotopes, *Nature Physics* **12**, 594 (2016).
- [60] G. Lalazissis, S. Karatzikos, R. Fossion, D. P. Arteaga, A. Afanasyev, and P. Ring, The effective force nl3 revisited, *Physics Letters B* **671**, 36 (2009).
- [61] S. Malbrunot-Ettenauer, S. Kaufmann, S. Bacca, C. Barbieri, J. Billowes, M. L. Bissell, K. Blaum, B. Cheal, T. Duguet, R. F. G. Ruiz, W. Gins, C. Gorges, G. Hagen, H. Heylen, J. D. Holt, G. R. Jansen, A. Kanellakopoulos, M. Kortelainen, T. Miyagi, P. Navrátil, W. Nazarewicz, R. Neugart, G. Neyens, W. Nörterhäuser, S. J. Novario, T. Papenbrock, T. Ratajczyk, P.-G. Reinhard, L. V. Rodríguez, R. Sánchez, S. Sailer, A. Schwenk, J. Simonis, V. Somà, S. R. Stroberg, L. Wehner, C. Wraith, L. Xie, Z. Y. Xu, X. F. Yang, and D. T. Yordanov, Nuclear charge radii of the nickel isotopes $^{58-68,70}\text{Ni}$, *Phys. Rev. Lett.* **128**, 022502 (2022).
- [62] O. Buss, T. Gaitanos, K. Gallmeister, H. van Hees, M. Kaskulov, O. Lalakulich, A. Larionov, T. Leitner, J. Weil, and U. Mosel, Transport-theoretical description of nuclear reactions, *Physics Reports* **512**, 1 (2012).
- [63] R. L. Workman and Others (Particle Data Group), Review of Particle Physics, *PTEP* **2022**, 083C01 (2022).
- [64] D. Atanasov, D. Beck, K. Blaum, C. Borgmann, R. Cakirli, T. Eronen, S. George, F. Herfurth, A. Herlert, M. Kowalska, S. Kreim, Y. Litvinov, D. Lunney, V. Manea, D. Neidherr, M. Rosenbusch, L. Schweikhard, F. Wienholtz, R. Wolf, and K. Zuber, Precision mass measurements of cesium isotopes—new entries in the ISOLTRAP chronicles, *Journal of Physics G: Nuclear and Particle Physics* **44**, 044004 (2017).
- [65] A. B. Larionov, I. A. Pshenichnov, I. N. Mishustin, and W. Greiner, Antiproton-nucleus collisions simulation within a kinetic approach with relativistic mean fields, *Phys. Rev. C* **80**, 021601 (2009).
- [66] A. B. Larionov, T. Gaitanos, and U. Mosel, Kaon and hyperon production in antiproton-induced reactions on nuclei, *Phys. Rev. C* **85**, 024614 (2012).
- [67] F. Grümmer, B. Chen, Z. Ma, and S. Krewald, Bulk properties of light deformed nuclei derived from a medium-modified meson-exchange interaction, *Physics Letters B* **387**, 673 (1996).
- [68] R. Panda, M. Sharma, and S. Patra, Nuclear structure and reaction properties of ne, mg and si isotopes with rmf densities, *Modern Physics Letters A* **29**, 1450013 (2014).
- [69] A. J. Miller, K. Minamisono, A. Klose, D. Garand, C. Kujawa, J. D. Lantis, Y. Liu, B. Maaß, P. F. Mantica, W. Nazarewicz, W. Nörterhäuser, S. V. Pineda, P.-G. Reinhard, D. M. Rossi, F. Sommer, C. Sumithrarachchi, A. Teigelhöfer, and J. Watkins, Proton superfluidity and charge radii in proton-rich calcium isotopes, *Nature Physics* **15**, 432 (2019).
- [70] H. Emrich, G. Fricke, G. Mallot, H. Miska, H.-G. Sieberling, J. Cavedon, B. Frois, and D. Goutte, Radial distribution of nucleons in the isotopes 48,40ca, *Nuclear Physics A* **396**, 401 (1983).
- [71] P. E. Hodgson, Nuclear matter distributions, *Hyperfine Interactions* **74**, 75 (1992).
- [72] J. Pochodzalla, S. Bleser, A. S. Lorente, M. M. Rojo, M. Steinen, for the PANDA Collaboration, J. Gerl, J. Kojouharova, and I. Kojouharov, Many facets of strangeness nuclear physics with stored antiprotons, in *Proceedings of the 12th International Conference on Hypernuclear and Strange Particle Physics (HYP2015)*, JPS Conference Proceedings

- (Journal of the Physical Society of Japan, 2017) p. 091002, <https://journals.jps.jp/doi/pdf/10.7566/JPSCP.17.091002>.
- [73] F. Schupp, *Study of antihyperon pairs in nuclei at PANDA*, Ph.D. thesis, Johannes Gutenberg-Universität Mainz ((unpublished)).
- [74] M. Steinen, *Feasibility studies for the high precision X-ray spectroscopy of heavy Ξ^- hyperatoms at PANDA using the PANda GERmanium Array PANGEA*, Phd thesis, Johannes Gutenberg-Universität Mainz ((2020)).
- [75] F. Schupp, M. Böltig, P. Achenbach, S. Bleser, J. Pochodzalla, and M. Steinen, An infrared light-guide based target positioning system for operation in a harsh environment, Nuclear Instruments and Methods in Physics Research Section A: Accelerators, Spectrometers, Detectors and Associated Equipment **1056**, 168684 (2023).
- [76] J. T. Zhang, X. L. Tu, P. Sarriuguren, K. Yue, Q. Zeng, Z. Y. Sun, M. Wang, Y. H. Zhang, X. H. Zhou, and Y. A. Litvinov, Systematic trends of neutron skin thickness versus relative neutron excess, Phys. Rev. C **104**, 034303 (2021).
- [77] Institut für Seltene Erden und Metalle AG, Price list of electromagnetically separated isotopes, <https://institut-seltene-erden.de/unser-service-2/metall-preise/preise-fuer-stabile-isotope/> (2023), accessed: 2023-04-30.
- [78] K. Suzuki, The \bar{p} physics opportunities at the j-parc hadron facility, <https://kds.kek.jp/event/46965/contributions/> (2024), fourth International Workshop on the Extension Project for the J-PARC Hadron Experimental Facility (HEF-ex 2024).
- [79] Christiansen, Martin, Schupp, Falk, Achenbach, Patrick, Böltig, Michael, Pochodzalla, Josef, and Steinen, Marcell, Exploring the neutron skin by hyperon-antihyperon production in antiproton-nucleus interactions, EPJ Web Conf. **271**, 02011 (2022).
- [80] M. Christiansen, *Einfluss der Neutronenhaut auf die Produktion von Hyperon-Anhyperon-Paaren bei Antiproton-Kern-Stößen*, Bachelor's thesis, Johannes Gutenberg-Universität Mainz (2022).
- [81] MOGON II High Performance Computing, <https://hpc.uni-mainz.de/>, accessed: 2024-11-18.
- [82] J. Lombardi, R. Boyd, R. Arking, and A. Robbins, Nuclear sizes in $^{40,44,48}\text{Ca}$, Nuclear Physics A **188**, 103 (1972).
- [83] I. Brissaud, Y. Le Bornec, B. Tatischeff, L. Bimbot, M. Brusssel, and G. Duhamel, Détermination du rayon de la distribution de neutrons de certains noyaux par l'étude de la diffusion élastique de particules alpha de 166 mev, Nuclear Physics A **191**, 145 (1972).
- [84] G. Alkhazov, T. Bauer, R. Bertini, L. Bimbot, O. Bing, A. Boudard, G. Bruge, H. Catz, A. Chaumeaux, P. Couvert, J. Fontaine, F. Hibou, G. Igo, J. Lugol, and M. Matoba, Elastic and inelastic scattering of 1.37 GeV α -particles from $^{40,42,44,48}\text{Ca}$, Nuclear Physics A **280**, 365 (1977).
- [85] M. J. Jakobson, G. R. Burleson, J. R. Calarco, M. D. Cooper, D. C. Hagerman, I. Halpern, R. H. Jeppeson, K. F. Johnson, L. D. Knutson, R. E. Marrs, H. O. Meyer, and R. P. Redwine, Neutron radii of calcium isotopes from pion total cross section measurements, Phys. Rev. Lett. **38**, 1201 (1977).
- [86] A. Chaumeaux, V. Layly, and R. Schaeffer, Neutron densities from 1 GeV proton scattering, Physics Letters B **72**, 33 (1977).
- [87] E. Friedman, H. J. Gils, H. Rebel, and Z. Majka, ^{48}Ca - ^{40}Ca Radius Difference from Elastic Scattering of 104-MeV α Particles, Phys. Rev. Lett. **41**, 1220 (1978).
- [88] G. Igo, G. Adams, T. Bauer, G. Pauletta, C. Whitten, A. Wreikat, G. Hoffmann, G. Blanquet, W. Coker, C. Harvey, R. Liljestrand, L. Ray, J. Spencer, H. Thiessen, C. Glashausser, N. Hintz, M. Oothoudt, H. Nann, K. Seth, B. Wood, D. McDaniels, and M. Gazzaly, Elastic differential cross sections and analyzing powers for $p+^{40,42,44,48}\text{Ca}$ at 0.8 GeV, Physics Letters B **81**, 151 (1979).
- [89] M. H. Mahzoon, M. C. Atkinson, R. J. Charity, and W. H. Dickhoff, Neutron skin thickness of ^{48}Ca from a nonlocal dispersive optical-model analysis, Phys. Rev. Lett. **119**, 222503 (2017).
- [90] V. E. Starodubsky and N. M. Hintz, Extraction of neutron densities from elastic proton scattering by $^{206,207,208}\text{Pb}$ at 650 MeV, Phys. Rev. C **49**, 2118 (1994).
- [91] A. M. Mack, N. M. Hintz, D. Cook, M. A. Franey, J. Amann, M. Barlett, G. W. Hoffmann, G. Pauletta, D. Ciskowski, and M. Purcell, Proton scattering by $^{206,207,208}\text{Pb}$ at 650 MeV: Phenomenological analysis, Phys. Rev. C **52**, 291 (1995).
- [92] B. Kłos and A. Trzcińska and J. Jastrzębski and T. Czosnyka and M. Kisielński and P. Lubiński and P. Napiorkowski and L. Pieńkowski and F. J. Hartmann and B. Ketzer and P. Ring and R. Schmidt and T. von Egidy and R. Smolańczuk and S. Wycech and K. Gulda and W. Kurcewicz and E. Widmann and B. A. Brown, Neutron density distributions from antiprotonic ^{208}Pb and ^{209}Bi atoms, Phys. Rev. C **76**, 014311 (2007).
- [93] Wycech, S. and Hartmann, F. J. and Jastrzębski, J. and Kłos, B. and Trzcińska, A. and Egidy, T. von, Nuclear surface studies with antiprotonic atom x rays, Phys. Rev. C **76**, 034316 (2007).
- [94] B. A. Brown, G. Shen, G. C. Hillhouse, J. Meng, and A. Trzcińska, Neutron skin deduced from antiprotonic atom data, Phys. Rev. C **76**, 034305 (2007).
- [95] Klimkiewicz, A. and Paar, N. and Adrich, P. and Fallot, M. and Boretzky, K. and Aumann, T. and Cortina-Gil, D. and Pramanik, U. Datta and Elze, Th. W. and Emling, H. and Geissel, H. and Hellström, M. and Jones, K. L. and Kratz, J. V. and Kulessa, R. and Nociforo, C. and Palit, R. and Simon, H. and Surówka, G. and Sümerer, K. and Vretenar, D. and Waluś, W. (LAND Collaboration), Nuclear symmetry energy and neutron skins derived from pygmy dipole resonances, Phys. Rev. C **76**, 051603 (2007).
- [96] A. Tamii, P. von Neumann-Cosel, and I. Poltoratska, Electric dipole response of ^{208}Pb from proton inelastic scattering: Constraints on neutron skin thickness and symmetry energy, The European Physical Journal A **50**, 28 (2014).
- [97] J. Piekarewicz, B. K. Agrawal, G. Colò, W. Nazarewicz, N. Paar, P.-G. Reinhard, X. Roca-Maza, and D. Vretenar, Electric dipole polarizability and the neutron skin, Phys. Rev. C **85**, 041302 (2012).
- [98] M. Csatlós and A. Krasznahorkay and D. Sohler and A.M. van den Berg and N. Blasi and J. Gulyás and M.N. Harakeh and M. Hunyadi and M.A. de Huu and Z. Máté and S.Y. van der Werf and H.J. Wörtche and L. Zolnai, Measurement of neutron-skin thickness in ^{208}Pb by excitation of the GDR via inelastic α -scattering, Nuclear Physics A **719**, C304 (2003).
- [99] A. Krasznahorkay, N. Paar, D. Vretenar, and M. Harakeh, Neutron-skin thickness of ^{208}Pb from the energy of the anti-analogue giant dipole resonance, Physica Scripta **T154**, 014018 (2013).
- [100] J. Yasuda, T. Wakasa, M. Okamoto, M. Dozono, K. Hatanaka, M. Ichimura, S. Kuroita, Y. Maeda, T. Noro, Y. Sakemi, M. Sasano, and K. Yako, Extraction of anti-analog giant dipole resonance and neutron skin thickness for ^{208}Pb , Progress of Theoretical and Experimental Physics **2013**, 10.1093/ptep/ptt038 (2013), <http://oup.prod.sis.lan/ptep/article-pdf/2013/6/063D02/19300640/ptt038.pdf>.

- [101] T. Wakasa, M. Okamoto, M. Dozono, K. Hatanaka, M. Ichimura, S. Kuroita, Y. Maeda, H. Miyasako, T. Noro, T. Saito, Y. Sakemi, T. Yabe, and K. Yako, Complete sets of polarization transfer observables for the $^{208}\text{Pb}(\vec{p},\vec{n})$ reaction at 296 MeV and Gamow-Teller and spin-dipole strengths for ^{208}Pb , *Phys. Rev. C* **85**, 064606 (2012).
- [102] T. E. Riley, A. L. Watts, S. Bogdanov, P. S. Ray, R. M. Ludlam, S. Guillot, Z. Arzoumanian, C. L. Baker, A. V. Bilous, D. Chakrabarty, K. C. Gendreau, A. K. Harding, W. C. G. Ho, J. M. Lattimer, S. M. Morsink, and T. E. Strohmayer, A NICER view of PSR j0030+0451: Millisecond pulsar parameter estimation, *The Astrophysical Journal* **887**, L21 (2019).
- [103] M. C. Miller, F. K. Lamb, A. J. Dittmann, S. Bogdanov, Z. Arzoumanian, K. C. Gendreau, S. Guillot, A. K. Harding, W. C. G. Ho, J. M. Lattimer, R. M. Ludlam, S. Mahmoodifar, S. M. Morsink, P. S. Ray, T. E. Strohmayer, K. S. Wood, T. Enoto, R. Foster, T. Okajima, G. Prigozhin, and Y. Soong, PSR j0030+0451 mass and radius from NICER data and implications for the properties of neutron star matter, *The Astrophysical Journal* **887**, L24 (2019).